J. Europ. Opt. Soc. Rap. Public. 9, 14032 (2014) www.jeos.org

Surface characterization by structure function analysis

T. Kreis Bremer Institut für angewandte Strahltechnik - BIAS, Klagenfurter Str. 2, D 28359 Bremen, Germany
kreis@bias.de

J. Burke Bremer Institut für angewandte Strahltechnik - BIAS, Klagenfurter Str. 2, D 28359 Bremen, Germany

R. B. Bergmann Bremer Institut für angewandte Strahltechnik - BIAS, Klagenfurter Str. 2, D 28359 Bremen, Germany

The structure function is a tool for characterizing technical surfaces which exhibits a number of advantages over Fourier-based analysis methods. So it is optimally suited for analyzing the height distributions of surfaces measured by full-field non-contacting methods. After the definition of line- and area-structure function and offering effective procedures for their calculation this tutorial paper presents examples using simulated and measured data of machined surfaces as well as optical components. Comparisons with the results of Fourier-based evaluations clearly prove the advantages of structure function analysis.
[DOI: http://dx.doi.org/10.2971/jeos.2014.14032]

Keywords: Surface measurement, surface representation, structure function, digital signal analysis

1 INTRODUCTION

The last decades have seen a rapid development of optical noncontacting metrology systems for measuring surface contours of technical components with high precision in the microscopic as well as in the macroscopic realms [1, 2]. For microscopic components the confocal scanning methods are state of the art [3]. For macroscopic objects most methods are based on the triangulation principle such as photogrammetric methods [4]. If patterns are projected, these may be points, as in the Shack-Hartmann methods [5], lines, grids, or even complex synthesized patterns in reverse engineering applications [6]. Fringes are projected onto the surface in Fourier-transform profilometry [7] or moire-techniques [8]. Specularly reflecting surfaces are measured by deflectometry [9, 10]. Interferometric methods like holographic contouring also find numerous application fields [11]. The resolution achievable by these methods can be further improved by using multiple redundant images employing phase-shifting [12] or Gray-code [13].

A common problem of all these metrologic methods is the handling of the raw data [5]. Normally the measured surface data are delivered as a point cloud which is stored in a suitable format in computer. But the utilization of the data for quality assurance purposes demands a representation of the data in a form appropriate for the problem to be solved. The questions to be answered by evaluation of the raw data can be manifold: In quality control one may be interested in the existence of defects such as holes, dents, bumps, scratches, or other flaws which normally manifest as localized high spatial frequency variations of the surface heights. On the other hand there may be interest in global criteria like e. g. periodicities, waviness, lay, or roughness.

Often Fourier-transform based methods are the first choice [14, 15]. So a few Fourier descriptors can indicate the existence of defects, or the power spectral density can describe global parameters of the measured surface data. Nevertheless the Fourier-approach exhibits severe drawbacks: Discontinuities at the edges of the sampling interval in 1D or 2D spread power all across the spectrum, an effect which is minimized by the application of window functions, like the well-known Hanning window. But this has the undesirable consequence that the measured samples enter the calculation of the spectra with unequal weights. Furthermore the 2D Fourier-transform assumes rectangular fields. In practice we often have arbitrary aperture shapes, so we can use zero-padding or choose a sub-aperture and assume it being sufficiently representative of the true surface characteristics. As a result we insert extrapolated data not really measured or discard measured values.

If the intention of our measurements is defect detection, a wavelet approach [16] was suggested as an alternative. If on the other hand one is more interested in the global criteria, the structure function is a suitable tool and will be presented in more detail in the following.

2 DEFINITION OF STRUCTURE FUNCTION

The structure function originally was introduced by Kolmogorov in 1941 for analysis of statistical problems associated with turbulence theory [17, 18]. In the meantime it found numerous applications in diverse fields: It was used for the characterization of technical surfaces [19], of optical surfaces [20, 21], of velocity fields in turbulent flows [17, 18, 22], and of phase and frequency instabilities in frequency sources [23], as well as for time series analysis in astronomy [24, 25], to name just a few.

Received April 04, 2014; resubmitted June 28, 2014; published August 15, 2014 ISSN 1990-2573

Let $f(\vec{x})$ be the measured data, which may be the height profile of a rough surface [19] or an optical surface [20, 21], a flow velocity [22], optical flux [25], optical phase differences [26] or similar data sets. Generally $f(\vec{x})$ can be treated as a random process. Then the structure function of order d is defined by $S_d(\vec{x'}-\vec{x}) = \langle(\delta f(\vec{x},\vec{x'}))^d\rangle$ with $\delta f(\vec{x},\vec{x'}) = |f(\vec{x}+\vec{x'}) - f(\vec{x})|$, see [22]. Most important and the only one used in the following is the structure function of order 2, so the subscript d will be omitted: $S = S_d$.

In detail, we have in one dimension the so called line structure function

$$S(x') = \int_{-\infty}^{\infty} [f(x) - f(x+x')]^2 dx. \tag{1}$$

If the $\vec{x} = (x, y)$ is two-dimensional, as e. g. the coordinates of a surface with heights $f(x, y)$, then the 2D structure function, also called area structure function, is

$$S(x', y') = \int_{-\infty}^{\infty}\int_{-\infty}^{\infty} [f(x,y) - f(x+x', y+y')]^2 \, dx \, dy. \tag{2}$$

To allow a meaningful comparison of the structure function in various spatial frequency bands, the normalized structure function $NSF(x)$ can be introduced [25]

$$NSF\{f\}(x') = \frac{S(x')}{\sigma^2}. \tag{3}$$

There are applications where the 1D line structure function suffices for evaluation of 2D data sets. Then each pixel pair is not represented by the pair of distances in each coordinate direction $(x_2 - x_1, y_2 - y_1)$ but only by the distance $\sqrt{(x_2 - x_1)^2 + (y_2 - y_1)^2}$. This already allows separation into characteristics like figure, roughness, and mid-spatial frequencies [21].

As an example we analyse a Zernike polynomial $Z_6^2(\rho, \phi)$, Figure 1(a). Several point pairs are indicated. They correspond to points along the line structure function, see Figure 1(b), as well as to points in the area structure function, see Figure 1(c), where due to redundancy only two quadrants are displayed. The colours in Figure 1 represent pixel differences: $(10, 10)$ in 2D corresponding to 14.14 in 1D (red); $(-8, 10)$ and 12.81 (green); $(0, 60)$ and 60 (violet); $(27, 0)$ and 27 (orange); $(-4, 4)$ and 5.66 (dark blue); $(-14, 14)$ and 19.80 (yellow).

3 CALCULATION OF THE STRUCTURE FUNCTION

In practice we are dealing with discrete measured data $\{f_i, i = 1, \ldots, I\}$. Then the structure function is calculated as

$$S(n) = \frac{1}{I - |n|} \sum_{i=\max\{1,1-n\}}^{\min\{I,I-n\}} (f_i - f_{i+n})^2$$
$$-N \le n \le N \tag{4}$$

with $N < I$. Due to the squaring we have an even structure function $S(-n) = S(n)$ for all n and also $S(0) = 0$, so it is not necessary to calculate redundant information and it suffices to determine the structure function only for positive differences n

$$S(n) = \frac{1}{I-n} \sum_{i=1}^{I-n} (f_i - f_{i+n})^2 \qquad n = 1, \ldots, N \tag{5}$$

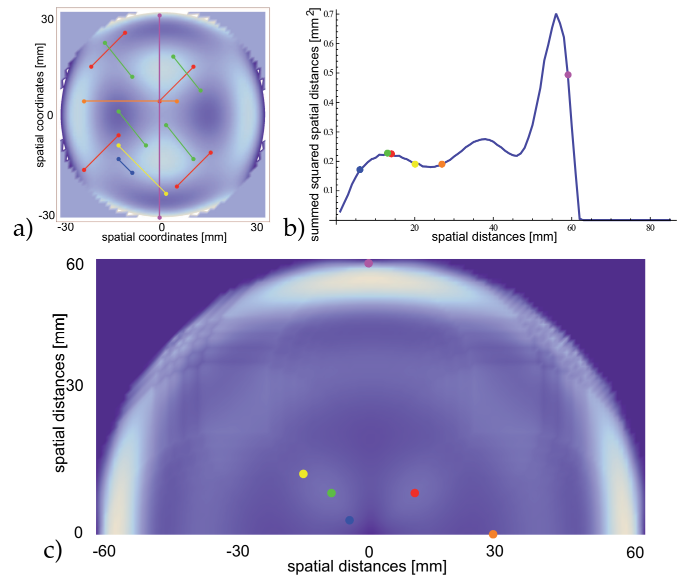

FIG. 1 a) Zernike polynomial $Z_6^2(\rho, \phi)$, b) line structure function, c) area structure function. Abscissa values: pixel coordinates in a), pixel differences in b) and c). Colours explained in text.

In two dimensions with $\{f_{i,j}, i = 1, \ldots, I, j = 1, \ldots, J\}$ we calculate the finite sum

$$S(n,m) = \frac{1}{I-|n|}\frac{1}{J-|m|} \times \sum_{i=\max\{1,1-n\}}^{\min\{I,I-n\}} \sum_{j=\max\{1,1-m\}}^{\min\{J,J-m\}} (f_{i+n,j+m} - f_{i,j})^2$$
$$-N \le n \le N$$
$$-M \le m \le M \tag{6}$$

with $N < I$ and $M < J$. This area structure function exhibits point symmetry $S(-n, m) = S(n, -m)$ for all n and m and also $S(0, 0) = 0$ so it suffices to calculate the area structure function in two quadrants. The parameters N and M are in the same range as the I and J and theoretically can be chosen up to $N = I - 1$, $M = J - 1$. But then for large n or m we average over only a few squared differences, so the determined values become unreliable due to noise and roughness. Therefore a choice of N and M as at most 80 % to 90 % of the magnitude of I and J is recommended.

It has to be mentioned that the calculation of $S(n, m)$ is not separable into a product of two sums, therefore the computational effort in the two-dimensional case is proportional to $I^2 J^2$ multiplications. In the case of 2D data sets to be analyzed with data value numbers in the range $I \times J = 10^3 \times 10^3$ this would lead to a number of floating-point multiplications proportional to $10^{12}/4$. A significantly lower number of multiplications is required by the following algorithm that also works for arbitrarily shaped apertures. Let $I = \max\{i\}$ and $J = \max\{j\}$ be the maximum numbers of points in i- and j-direction and assume a rectangle of $I \times J$ measured values, that contains all actually measured points. Then the algorithm works as follows:

- The rectangle of the $I \times J$ measured pixels is divided into $I' \times J'$ subareas, each of the same of length about 10×10 measured values.

- For each of these subareas we initialize its sum by zero and also its count by zero.
- Using a random number generator we select a random pair of points. If one of these points falls outside the aperture, the random selection is repeated.
- The distance vector $\vec{r}$ between these two points is calculated.
- We calculate the squared difference of the measured values at the two points.
- The subarea containing vector $\vec{r}$ gets its sum increased by the just calculated squared difference and its count increased by one.
- The steps beginning with the random choice of a point are repeated about 10^5 to 10^6 times.
- Finally for each subarea its cumulated sum is divided by its cumulated count.

This algorithm determines an area structure function which approximates the averaged exact area structure function, where averaging is performed over rectangles of size $(I/I') \times (J/J')$. Due to the random choice of point pairs, small differences will occur more frequently. Thus the approximation is highly reliable for differences close to zero, but becomes noisy when approaching large differences, requiring both randomly chosen points to be positioned at opposite ends in the measurement aperture, see results in Section 5. The big advantage is the significant decrease of the number of multiplications which is of the order of 10^3 to 10^4, see Section 5.

4 PROPERTIES OF THE STRUCTURE FUNCTION

For statistically stationary processes the structure function $S(\vec{x})$ of order 2 is related to the autocovariance function $R(\vec{x})$ by $S(\vec{x}) = 2[R(0) - R(\vec{x})]$ [19]. It contains the same information as the autocovariance function and its Fourier transform, the power spectral density function, but offers some practical advantages: it is stable and easy to compute, it does not impose a periodogram model on the measured surface, and it avoids the singularity at the origin of the autocovariance function [19]. Also the structure function can be related to the autocorrelation function $\phi_{ff}(x')$: Let σ^2 be the variance of the underlying stochastic process then $S(x) = 2\sigma^2[1 - \phi_{ff}(x)]$, see Appendix A. Although the structure function thus carries principally the same information as the power spectral density function, it does not have the disadvantages of the Fourier-transform based indicators named in the Introduction. The structure function can easily deal with arbitrary apertures and does not need any windowing. A more general approach to the structure function is given in Appendix B.

The structure function has a minimal value of 0 at pixel distance zero, $S(0) = 0$. This corresponds to the maximum of the autocorrelation function at zero, $\phi_{ff}(0) = 0$. The squaring in the calculation of S_2 causes the evenness of S_2, so the 1D structure function $S_2(x')$ normally is only used for positive pixel distances $x' \geq 0$.

The advantages of the structure function approach compared to Fourier-based methods are pointed out in the next example, Figure 2. We assume an irregularly shaped surface which furthermore shows a hole, Figure 2(a). In practice it does not matter whether this hole physically exists or only represents corrupted data which are to be excluded from evaluation. In Figure 2(a) bright area represents surface data points, dark stands for no data. This results in possible and impossible point pair distances. Figure 2(b) displays the first quadrant of the plane of point pair distances indicating possible pairs in bright, impossible pairs in dark. E. g. for the distance (400,100), represented in red, no valid point pair can be found in Figure 2(a). Three point pairs with distance (400,100) are given in Figure 2(a), none with both endpoints can be found inside the surface. On the other hand point pair distance (90,250) shown in green is a possible one, also three point pairs for this distance are drawn into Figure 2(a).The simulated measurement values describe a cosine-valued displacement $A\cos(f\pi x)$ with $A = 1.5$, $f = 0.038$ and the x-coordinate along the horizontal axis, Figure 2(c). The resulting area structure function can be seen in Figure 2(d). It reflects the periodic nature of the displacement function in horizontal direction as expected. Only at the margins of the allowed area can higher fluctuations be seen. For these distances only a few pixel pairs can be found in the measured data, so errors are not compensated by averaging a high number of measured points. For comparison purposes a Fourier based evaluation was performed. The pixels outside the surface were given the value zero to fill the full 512×512-pixel square - the common zero padding. The Fourier transform $F(u,v) = \mathcal{F}\{f(x,y)\}$ of this real distribution is calculated employing the FFT-procedure and the power spectral density $S(u,v)$ is derived pointwise by $S(u,v) = F(u,v)F^*(u,v)$. We then obtained the autocorrelation $\phi_{ff}(x,y)$ by applying the inverse Fourier transform $\phi_{ff}(x,y) = \mathcal{F}^{-1}\{S(u,v)\}$ where the x,y can be interpreted as shifts or point pair distances. $1.0 - \phi_{ff}(x,y)$ is given in Figure 2(e), it should be proportional to the structure function, Figure 2(d). For better visual comparison this distribution of Figure 2(e) is masked by the values 1. and 0. of Figure 2(b) and in the resulting Figure 2(f) we recognize severe differences to Figure 2(d), which result from aliasing and zero padding in the Fourier approach. The advantages of structure function evaluation are therefore obvious.

5 APPLICATION OF THE STRUCTURE FUNCTION

Figure 3 shows an example from practice, a measured height profile of 445×403 points. As can be seen in the gray-scale display, only values in a rectangular, inclined aperture are measured. The height-values along a single column, here arbitrarily the one with index 201, are extracted, see Figure 4. Along this line the 1D structure function is calculated with parameters $I = 445$ and $N = 400$, see Figure 5. This line structure function starts with zero at the origin and has a local minimum at a displacement of about 175 pixels, and two local

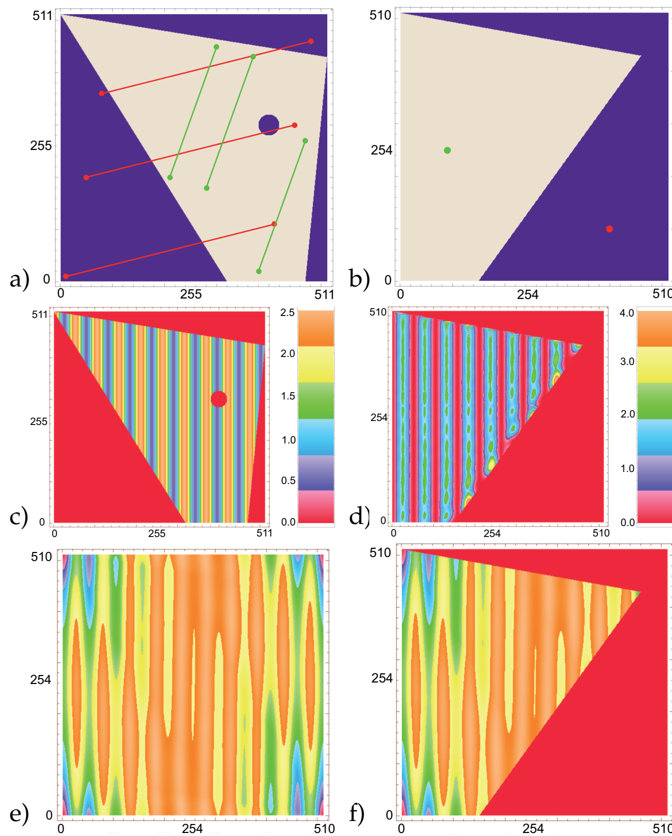

FIG. 2 a) Contour of measured surface, bright: surface points; dark: no surface (red/green lines: see text); b) possible (bright) and impossible (dark) point pair distances; c) simulated displacement; d) area structure function; e) negative of autocorrelation function; f) negative of autocorrelation masked to possible point pair distances

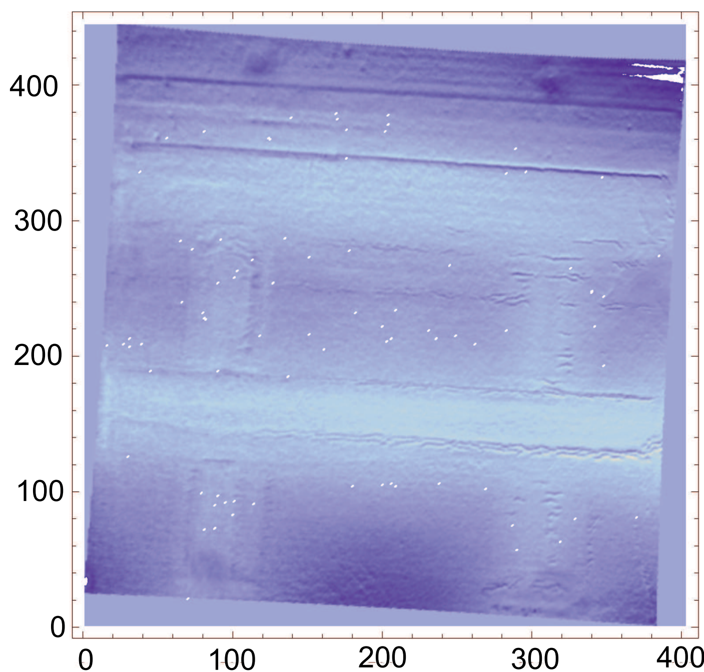

FIG. 3 Gray scale display of measured values, units: pixel numbers corresponding to spatial coordinates

maxima at about 100 and about 275 pixels. The local minimum indicates small squared differences, thus similar structures in the gray scale image of the measured values which have a distance of about 175 pixels. This is pointed out in Figure 6

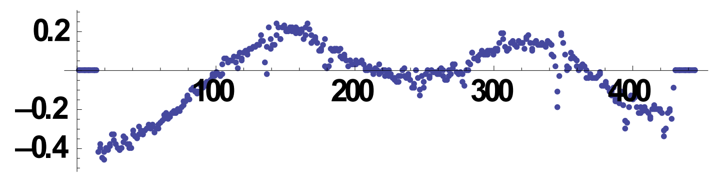

FIG. 4 Measured values along column 201 in Figure 3, abscissa: pixel numbers (spatial coordinate), ordinate: height values [mm]

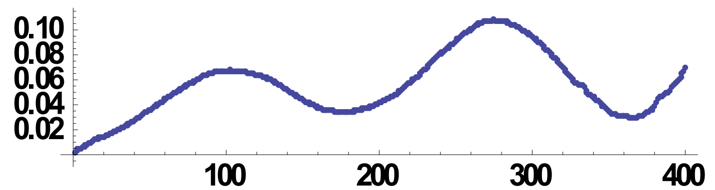

FIG. 5 Line structure function along column 201 Figure 3, abscissa: pixel number differences, ordinate: structure function values [mm^2]

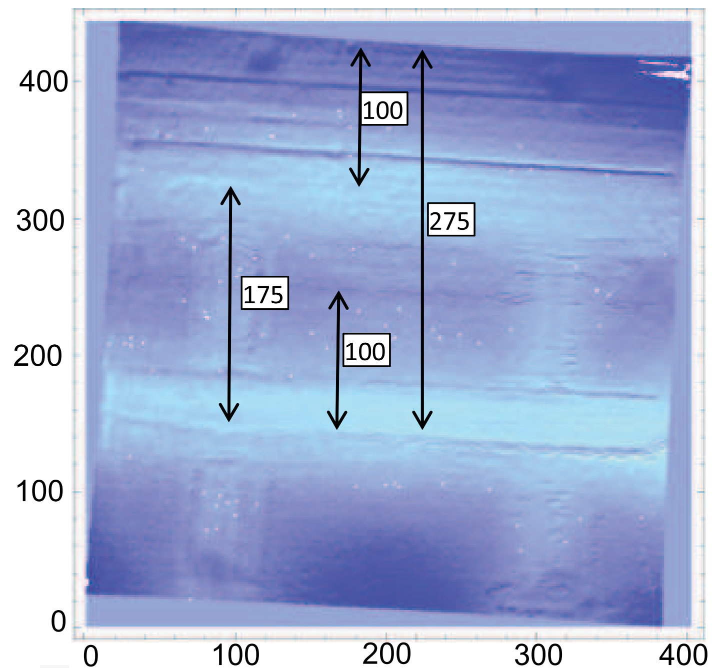

FIG. 6 Distances of different (100 and 275) and repeating (175) structures in the data set

by the double arrow marked by 175. This value can be interpreted as period of the waviness of the surface. The local maxima indicate large squared differences corresponding to half-numbered periods if we assume nearly harmonic functions. The two-dimensional area structure function of the whole 2D data file calculated by the algorithm given above is shown in Figure 7. The whole picture of $I \times J = 445 \times 403$ pixels was subdivided into $I' \times J' = 45 \times 41$ subareas of 10×10 pixels, resulting in a discrete area structure function of 90×82 values due to positive as well as negative $\vec{r}$. The number of the cumulated squared differences has been varied to a) 10000, b) 50000, c) 100000, d) 500000 randomly chosen pairs of points. If a pair was selected with at least one of the points lying outside the object, this pair was excluded from computation. Instead of more than 10^{10} multiplications we have used fewer than 10^6 multiplications when calculating the area structure function shown in Figure 7(d). Nevertheless we obtain a smooth

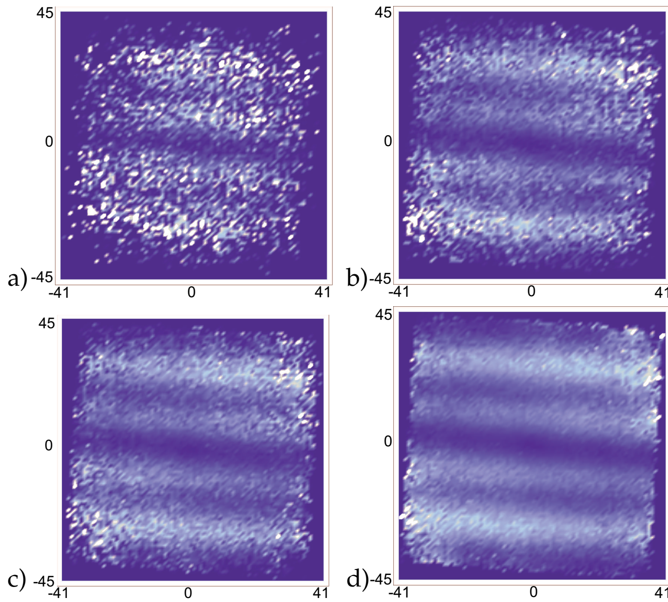

FIG. 7 Area structure function calculated with a) 10000, b) 50000, c) 100000, d) 500000 pairs of points. Distance pair (0,0) in the center of each display.

and meaningful approximation, at least at all point pairs not too close to the margins. Figure 7 clearly demonstrates the decreasing noise when increasing the number of randomly chosen pairs. The long spatial wavelength components in vertical direction in the measured surface can be recognized in the area structure function of Figure 7. The appearance of parallel fringes in the area structure function gives strong evidence that the detected waviness is a global one, it does not vary from one column to another. There is no direct correlation between the local amplitudes of the area structure function and the height of the waviness in the measured data. But due to its integrating nature the structure function will detect regular patterns like lay or waviness even if these are embedded in noise, which may be generated by surface roughness or speckles, if coherent light was used for measurement. Furthermore in the interpretation of Figure 7 one has to pay attention to the subarea size: the numbering along the axes relates to this subarea size. In our example we have chosen subareas of 10×10 pixels, so the large differences at distances 100 and 275 indicated in Figure 6 are reflected at subarea distances of 10 and 27.5.

The next example is from characterization of optical components. Here usually the transmitted optical wave fronts are investigated, so we must analyse the structure of optical phase distributions. If the exit pupil of an optical system to be tested is circular, which is the case in most applications, then the aberrations present in the system can be represented in terms of Zernike polynomials. These are orthogonal and normalized within a circle of unit radius [27]. Then the phase error $\phi_A(x, y)$ is represented by an expansion into the Zernike polynomials $Z_k(\rho, \phi)$ where ρ is the radial coordinate within the unit circle and ϕ is the polar angle. Each Zernike polynomial is of the form $Z_n^m(\rho, \phi) = R_n^m(\rho) \cos(m\phi)$ with

$$R_n^m(\rho) = \begin{cases} \sum_{k=0}^{(n-m)/2} \frac{(-1)^k (n-k)!}{k![(n+m)/2-k]![(n-m)/2-k]!} & : n-m \text{ even} \\ 0 & : n-m \text{ odd} \end{cases} \quad (7)$$

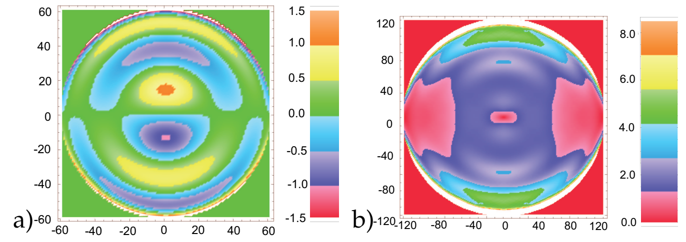

FIG. 8 a) Zernike polynomial $Z_7^1(\rho, \phi)$. b) Corresponding area structure function

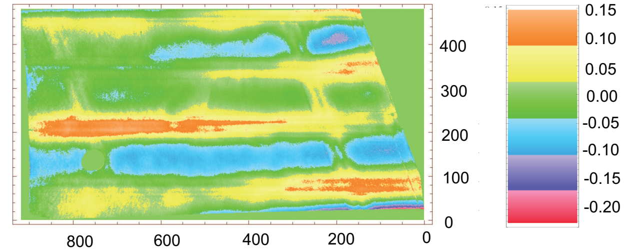

FIG. 9 Measured surface height data of airplane wing section

Thus $\phi_A(\rho, \phi)$ can be written [27]

$$\phi_A(\rho, \phi) = \sum_{k=1}^{K} w_k Z_k(\rho, \phi) \quad (8)$$

and the root-mean square error $\overline{\phi_A}$ due to aberrations is

$$\overline{\phi_A} = \sqrt{\sum_{k=K+1}^{\infty} w_k^2} \quad (9)$$

As He et al [21] pointed out, the residual error in $\phi_A(\rho, \phi)$ can be determined by subtracting the first K Zernike terms, then this error should be analyzed by the area structure function for detecting e. g. ripples.

Figure 8(a) shows the Zernike polynomial $Z_7^1(\rho, \phi)$ and Figure 8(b) displays its area structure function. While the Zernike polynomial $Z_7^1(\rho, \phi)$ is odd in the vertical direction, its corresponding area structure function by principle is even in the horizontal as well as in the vertical direction. He et al [20, 21] have pointed out the capability of the area structure function for detecting surface anisotropy and distinguishing different error geometries when investigating measured phase distributions, while the line structure function does not exhibit this ability.

Figure 9 gives the last example, the height distribution along an airplane wing section measured by fringe projection. We observe that the wing section does not fill the full rectangular area of 919×481 measurement points. Especially there is a hole which is clearly seen in the mask image of Figure 10 with all measurement points marked white and the points with no measured value marked black. Here we have a typical example of a non-rectangular aperture. First we calculate all 1D line structure functions along the columns, see Figure 11. The columns are numbered from 1 to 919 along the abscissa, while along the ordinate we have spatial differences, the arguments of the structure functions. For the low numbered columns the structure function values of large differences are lacking, because due to the non-rectangular aperture there do not exist

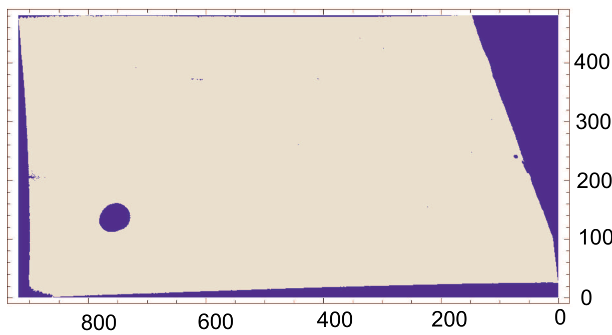

FIG. 10 Mask image. White: measured point; black: no measurement

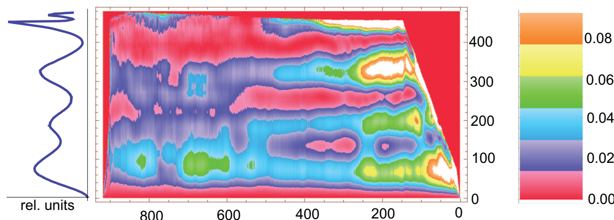

FIG. 11 1D-structure function along all columns and integrated values along all line coordinates (left). Abscissa: spatial coordinates; ordinate: spatial differences. Only positive spatial differences.

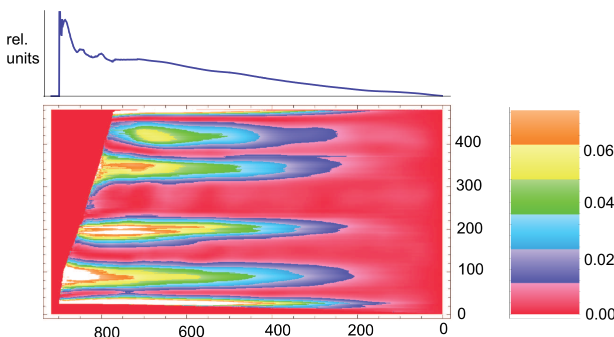

FIG. 12 1D-structure function along all lines (below) and averaged values along all column coordinates (above) . Abscissa: spatial differences; ordinate: spatial coordinates. Only positive spatial differences.

two measured points far apart. The same effect, but not as pronounced as before, is seen for the high numbered columns. Local minima appear at differences around 130, 260 and 390 pixels, which indicates a waviness with a periodicity around 130 pixels. This also is made obvious in the average of all these line structure functions displayed at the left of Figure 11. The outliers at point differences higher than 420 are due to the fact that there is averaging over only very few point pair differences.

The 1D line structure functions along all lines are shown in Figure 12. Here no distinct local minima are present in the structure functions, neither in the integral over all line structure functions displayed above, nor locally in the individual line structure function. Thus no waviness in horizontal direction is detected. Nevertheless we observe increasing amplitudes with increasing differences (from right to left) in the integrated structure function. This indicates a slight overall tilt of the measured structure, which can be eliminated before the structure function calculation, see Section 6.

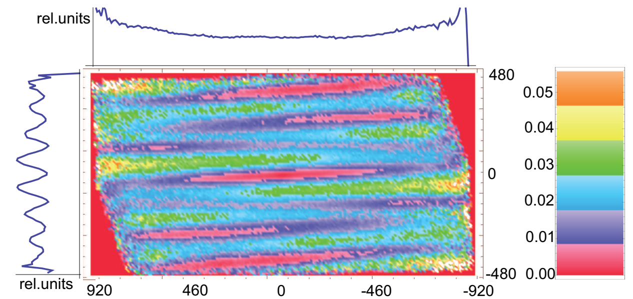

FIG. 13 2D-structure function and integrated values along all line (left) and column coordinates (above). Abscissa and ordinate: spatial differences. Positive and negative differences of spatial positions in each direction.

The area structure function calculated using 5×10^6 randomly chosen point pairs is given in Figure. 13. Especially the average structure function gained by integration over all lines or columns, confirm the aforementioned statements regarding the waviness. The area structure function in Figure 13 is approximately point symmetric. It is not perfectly point symmetric, since due to the stochastic choice of point pairs not for each point pair $((x_1, y_1), (x_2, y_2))$ also the corresponding symmetric pair $((x_2, y_2), (x_1, y_1))$ is used for calculation. This procedure maps each point difference into the corresponding one of the four quadrants. A better procedure would be the calculation of the 2D structure function in only two quadrants, thus using in the average twice as many samples at each point difference of the structure function.

6 STRUCTURE FUNCTION AND FILTERING

Generally the form of the structure function is influenced by an uneven background in the data set. In many cases the measured underlying background of a plane surface is a linear function due to a tilt of the surface, a parabolic function indicating a bending, or a bellshaped curve caused by irregular illumination when using optical intensity based measurement methods, to name just a few. The effect of determining such background by linear regression and removing it before calculating the structure function is shown in Figures 14 to 16. The measured heights of a rectangular surface are displayed as gray values in Figure 14. The heights along a central line are given in Figure 15. A cubic function describing a global deformation is fitted by linear regression, Figure 16(a), the differences of the heights from this parabola are shown in Figure 16(b). The structure function calculated from the original values is displayed in Figure 16(c), while the structure function of the heights without background can be seen in Fig. 16(d). The dissimilarity between Figures 16(c) and d can be interpreted as follows: The difference between the first left maximum and the rightmost local minimum is amplified by the uneven background. This difference is reflected in the structure function as a local maximum near a 360 pixel shift, the right local maximum in Figure 16(c). In contrast, the left local maximum is the higher one in Figure 16(d), resembling the differences between neighboring opposite local extrema in Figure 16(b). The measured values exhibit a waviness with a period of about 260 pixels. This is seen in Figure 16(d) as a central local minimum. As a consequence one must conclude that

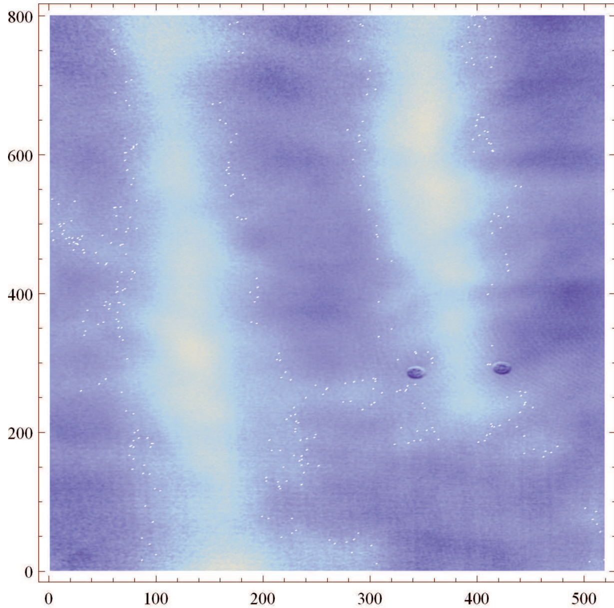

FIG. 14 Measured surface heights in 801×519 pixels

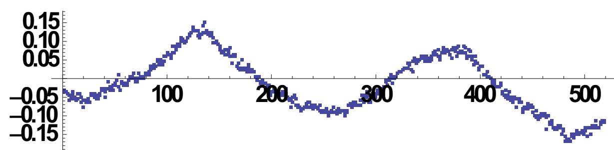

FIG. 15 Measured surface heights along line 401 in Figure 14

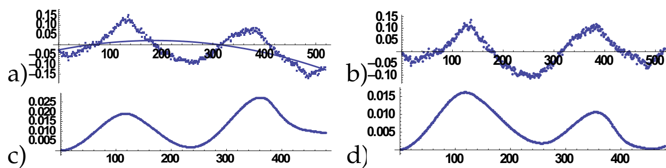

FIG. 16 Calculation of structure function. (a) measured data with fitted parabola. (b) Data after removing background. (c) Structure function of data without background removal. (d) Structure function calculated after background removal.

a previous background correction yields more reliable structure functions and thus is strongly recommended.

The background elimination can be viewed as a sort of highpass-filtering. It has to be applied judiciously depending on the spatial frequencies of interest. Furthermore one has to keep in mind that each value of $S(n)$ is an average over $I - n$ differences or a subset thereof. So for rough surfaces the values $S(n)$ for small n are more reliable than those for large n. This effect can be diminished by a low-pass-filter with a cutoff-frequency chosen to eliminate the high-frequency surface height fluctuations due to roughness.

7 CONCLUSION AND OUTLOOK

In this paper we have defined and analyzed the structure function and have shown its ability to characterize surfaces whose height distribution is measured by one of the numerous optical noncontacting methods. Various ways to extract 1D structure function information from the 2D height distribution have been demonstrated, some of them - those averaging pointwise over all line structure functions - for the first time. The advantages of the structure function compared to Fourier-based approaches have been pointed out and shown by example. Especially if the contour of the measured surface is not rectangular or if the continuation at the surface's margins is not smooth, then the structure function approach has to be favoured, since it exhibits no leakage nor aliasing. The structure function's applicability is demonstrated by simulated as well as practically measured examples like surface height variations or optical phase distributions. We have seen that the positions of local extrema indicate precisely the existence or non-existence of waviness as well as its spatial frequency. What is still lacking, is a general procedure to draw significant parameters from the structure function which characterize the investigated surface, such as indicating and quantifying lay, waviness, slope, roughness and other parameters. Although the emphasis of the paper was on evaluation of optically measured height distributions, the capability of the structure function approach to phase error characterization in the testing of optics also was mentioned. The results regarding the structure function presented in this paper should draw the attention of those analyzing technical or optical surfaces to structure function analysis and its manifold capabilities.

8 ACKNOWLEDGEMENTS

The authors thank Alan McMillan of GKN Aerospace for providing access to the wing sections for measurement. Parts of the investigations have been supported by the EU in the framework of the Clean Sky programme under JTI-CS-2010-5-SFWA-03-004 Grant Agreement 286745 which is gratefully acknowledged.

A APPENDIX

Let $f(x)$ be a stationary random variable and $\phi_{ff}(x')$ the related autocorrelation function. Then

$$S(x) = 2\sigma^2[1 - \phi_{ff}(x)] \tag{10}$$

Proof: Let $R(x') = \langle f(x)f(x+x')\rangle$ be the autocovariance function, then due to stationarity

$$\langle f^2(x)\rangle = \langle f^2(x+x')\rangle = R(0) = \sigma^2 \tag{11}$$

Thus

$$\begin{aligned} S(x') &= \langle [f(x) - f(x+x')]^2\rangle \\ &= \langle f^2(x)\rangle + \langle f^2(x+x')\rangle + 2\langle f(x)f(x+x')\rangle \\ &= R(0) + R(0) - 2R(x') = 2\sigma^2 - 2\sigma^2\frac{R(x')}{\sigma^2} \\ &= 2\sigma^2[1 - \phi_{ff}(x')] \end{aligned} \tag{12}$$

B APPENDIX

Rutman [23] defines the structure function by the increment of a random process: Let $g(t)$ be a random process. For $M \geq 1$ the Mth increment of this process is defined by

$$\Delta^{(M)}g(t;\tau) = \sum_{k=0}^{M}(-1)^k\binom{M}{k}g(t+(M-k)\tau) \tag{13}$$

The process $g(t)$ has a stationary Mth increment, if the following averages exist for all real T and τ and do not depend on the instant t:

$$\begin{aligned} \langle \Delta^{(M)} g(t;\tau) \rangle &= \alpha(\tau) \\ \langle \Delta^{(M)} g(t;\tau) \cdot \Delta^{(M)} g(t+T;\tau) \rangle &= D_g^{(M)}(T;\tau) \end{aligned} \quad (14)$$

In other words, the Mth increment has a time independent mean and its autocorrelation depends only on the time difference T (wide sense stationarity) [23].

By definition $D_g^{(M)}(T;\tau)$ is the structure function of the Mth increment. The Mth structure function of the random process $g(t)$ is defined as $D_g^{(M)}(\tau) = D_g^{(M)}(T=0;\tau)$:

$$D_g^{(M)}(\tau) = \langle [\Delta^{(M)} g(t;\tau)]^2 \rangle \quad (15)$$

Special case: The 1st increment of the random process $g(t)$ is

$$\begin{aligned} \Delta^{(1)} g(t;\tau) &= \sum_{k=0}^{1} (-1)^k \binom{1}{k} g(t+(1-k)\tau) \\ &= (-1)^0 \binom{1}{0} g(t+(1-0)\tau) \\ &+ (-1)^1 \binom{1}{1} g(t+(1-1)\tau) \\ &= g(t+\tau) - g(\tau) \end{aligned} \quad (16)$$

So the 1st structure function of the process is

$$D_g^{(1)}(\tau) = \langle [\Delta^{(1)} g(t;\tau)]^2 \rangle = \langle [g(t+\tau) - g(\tau)]^2 \rangle \quad (17)$$

which coincides with our previous definition of the structure function.

References

[1] R. Bergmann, and Ph. Huke, "Advanced Methods for Optical Nondestructive Testing" in W. Osten, and N. Reingand (eds.): *Optical Imaging and Metrology* (Wiley-VCH, Weinheim, 2012).

[2] E. Savio, L. De Chiffre, and R. Schmitt, "Metrology of freeform shaped parts," CIRP Ann.-Manuf. Techn. **56**(**2**), 810–835 (2007).

[3] D. M. Shotton, "Electronic light microscopy: present capabilities and future prospects,"Histochem. Cell Biol. **104**, 97–137 (1995).

[4] H. Schwenke, U. Neuschaefer-Rube, T. Pfeifer, and H. Kunzmann, "Optical Methods for Dimensional Metrology in Production Engineering," CIRP Ann.-Manuf. Techn. **51**(**2**), 685–699 (2002).

[5] T. Yoshizawa (Ed.), *Handbook of Optical Metrology* (CRC Press, Boca Raton, 2009).

[6] J. Burke, T. Bothe, W. Osten, and C. Hess, "Reverse Engineering by Fringe Projection," Proc. SPIE **4778**, 312–324 (2002).

[7] X. Su, W. Chen, Q. Zhang, and Y. Chao, "Dynamic 3-D shape measurement method based on FTP," Opt. Laser Eng. **36**(**1**), 49–64 (2001).

[8] O. Kafri, and I. Glatt, *The Physics of Moire Metrology* (Wiley Series in Pure Applied Optics, New York, 1990).

[9] J. Burke, W. Li, A. Heimsath, C. von Kopylow, and R. Bergmann, "Qualifying parabolic mirrors with deflectometry," J. Europ. Opt. Soc. Rap. Public. **8**, 13014 (2013).

[10] T. Bothe, W. Li, C. v. Kopylow, and R. Bergmann. "The Fringe Reflection Technique for Lens Inspection and Specular Freeform Measurement," MAFO Ophthalmic Labs & Industry **5**, 38–42 (2009).

[11] Th. Kreis, *Handbook of Holographic Interferometry* (Wiley-VCH, Weinheim, 2005).

[12] Y. Hu, J. Xi, J. Chicharo, and Z. Yang, "Improved Three-Step Phase Shifting Profilometry Using Digital Fringe Pattern Projection," in *Proceedings of International Conference on Computer Graphics, Imaging and Visualisation*, 161–167 (IEEE, Sydney, 2006).

[13] G. Sansoni, S. Corini, S. Lazzari, R. Rodella, and F. Docchio, "Three-dimensional imaging based on Gray-code light projection: characterization of the measuring algorithm and development of a measuring system for industrial applications," Appl. Optics **36**(**19**), 4463–4472 (1997).

[14] J. Sijbers, T. Ceulemans, and D. van Dyck, "Algorithm for the computation of 3D Fourier descriptors," in *Proceedings of International Conference on Pattern Recognition (ICPR'02)*, 20790 (IEEE Computer Society, Quebeck, 2002).

[15] M.-F. Wu, and H.-T. Sheu, "Representation of 3D surfaces by two-variable Fourier descriptors," IEEE T. Pattern Anal. **20**(**8**), 858–863 (1998).

[16] L. Rosenboom, Th. Kreis, and W. Jüptner, "Surface description and defect detection by wavelet analysis," Meas. Sci. Technol. **22**(**4**), 045102 (2011).

[17] A. N. Kolmogorov, "The local structure of turbulence in incompressible viscous fluids at very large Reynolds numbers (in Russian)," Dokl. Akad. Nauk. SSSR **30**, 299–303 (1941).

[18] A. N. Kolmogorov, "Dissipation of energy in isotropic turbulence (in Russian)," Dokl. Acad. Nauk. SSSR **32**, 19–21 (1941).

[19] T. R. Thomas, B.-G. Rosen, and N. Amini, "Fractal characterization of the anisotropy of rough surfaces", Wear **232**, 41–50 (1999).

[20] L. He, A. Davies, and C. J. Evans, "Comparison of the area structure function to alternate approaches for optical surface characterization," Proc. SPIE **8493**, (2012).

[21] L. He, C. J. Evans, and A. Davies, "Two-quadrant area structure function analysis for optical surface characterization," Opt. Express **20**(**21**), 23275–232801 (2012).

[22] P. L. Vanyan, "Structure function of the velocity field in turbulent flows," JETP **82**(**3**), 580–586 (1996).

[23] J. Rutman, "Characterization of Phase and Frequency Instabilities in Precision Frequency Sources: Fifteen Years of Progress", Proc. IEEE **66**(**9**), 1048–1075 (1978).

[24] J. H. Simonetti, J. M. Cordes, and D. S. Heeschen, "Flicker of extragalactic radio sources at two frequencies," Astrophys. J. **296**, 46–59 (1985).

[25] B. Czerny, V. T. Doroshenko, M. Nikolajuk, A. Schwarzenberg-Czerny, Z. Loska, and G. Madejski, "Variability of accretion flow in the core of the Seyfert galaxy NGC4151," Mon. Not. R. Astron. Soc. **342**, 1222–1240 (2003).

[26] A. M. Hvisc, J. H. Burge, "Structure function analysis of mirror fabrication and support errors," Proc. SPIE. **66710A** (2007).

[27] O. K. Ersoy, *Diffraction, Fourier Optics and Imaging* (J. Wiley and Sons, New Jersey, 2007).